Molecular Crystals and Liquid Crystals

Publication details, including instructions for authors and subscription information:
http://www.tandfonline.com/loi/gmcl20

Universal Features in the Nematic Uniaxial-to-Biaxial Transition

Fulvio Bisi [a]

[a] Dipartimento di Matematica and CNISM, Università di Pavia, Pavia, Italy

Version of record first published: 30 Jan 2009

To cite this article: Fulvio Bisi (2008): Universal Features in the Nematic Uniaxial-to-Biaxial Transition, Molecular Crystals and Liquid Crystals, 495:1, 112/[464]-132/[484]

To link to this article: http://dx.doi.org/10.1080/15421400802430547

Mol. Cryst. Liq. Cryst., Vol. 495, pp. 112/[464]–132/[484], 2008

ISSN: 1542-1406 print/1563-5287 online
DOI: 10.1080/15421400802430547

Taylor & Francis
Taylor & Francis Group

Universal Features in the Nematic Uniaxial-to-Biaxial Transition

Fulvio Bisi
Dipartimento di Matematica and CNISM, Università di Pavia, Pavia, Italy

Recent experimental findings about new nematogenic molecules have reported thermally driven transitions to biaxial phases, which has revived the interest for macroscopic biaxiality. In particular, the simplified interaction model proposed by Straley for molecules endowed with D_{2h} symmetry has met renewed interest. In the scenario obtained for phases a unifying character can be captured. There exists a universal feature in the behaviour of one uniaxial order parameter, rebounding at the biaxial-to-uniaxial transition. This finding has been confirmed by means of a Monte-Carlo simulation. Moreover, the phase sequences and the order of the transitions are poorly influenced by one of the interaction parameters.

Keywords: biaxial; minimax principle; nematic liquid crystal

1. INTRODUCTION

The theoretical prediction of nematic biaxial phases in thermotropic liquid crystals by Freiser [1,2] dates back to the early '70s. Whilst very soon after Freiser papers Yu and Saupe [3] gave experimental proof of

First of all, I need to acknowledge E. G Virga, G. De Matteis and S. Romano; this paper is based on the fruit of our collaboration. I am indebted to E. C. Gartland, Jr. for precious suggestions and enlightening discussions on the mean-field bifurcation analysis adopted in this paper, during our common stay at the IMA, Institute for Mathematics and its Applications, University of Minnesota, Minneapolis MN (USA), where part of this work was done. Financial support from both the Royal Society of London through the Project *Biaxial liquid crystals: mathematical models and simulation* and the Italian Ministry for Higher Education MIUR through the PRIN Grant No. 2004024508 is gratefully acknowledged. Last, but absolutely not least, my gratitude goes to G. R. Luckhurst, who prompted some of the exploration presented in this paper.

Address correspondence to Fulvio Bisi, Dipartimento di Matematica and CNISM, Università di Pavia, Via Ferrata 1, Pavia 27100, Italy. E-mail: fulvio.bisi@unipv.it

the existence of biaxial phases in lyotropic liquid crystals, thermally driven transitions to biaxial phases have proved far more elusive than expected, and the quest for thermotropics has experienced alternate luck [4]. Recently several independent observations of such phases [5–10] have renewed interest among liquid crystal experts [11]; however, these experimental results do not yet meet with unanimous consensus [12–14].

Details of the analytical and computational methods supporting the existence of thermotropic biaxial phases can be found elsewhere, for example, in [15]; however, the main issues will be resumed here for the sake of completeness and for later reference. First, one has to record the mean-field model originally put forward by Straley [16,17] and the detailed Monte Carlo simulation performed by Biscarini *et al.* [18] employing a particular instance of Straley's pair-potential, related to the London dispersion forces approximation [19]. Excluded-volume models have been investigated as well; a prediction of a biaxial phase can be obtained in this case for appropriate choices of potentials [20–24]. Another mean-field model has its foundations in a different realisation of Straley's pair-potential [25,26]; this model revealed the possibility for the direct isotropic-to-biaxial transition to take place over a full range of model parameters, instead of a single one, as opposite to the dispersion forces approximation. Moreover, according to this model the transition to the biaxial phase from both isotropic and uniaxial phases can be either first- or second-order, depending on the choice of a model parameter [27,28]. Finally, Straley's general pair-potential has recently been studied [30] for all inequivalent choices of the model parameters [29].

Straley's interaction Hamiltonian H can always be decomposed as the sum of two London interactions, but they need not be both attractors [30], which, on the contrary, is the case of dispersion forces approximation. When the region of admissible Straley's parameters is considered in our parametrisation, a parabola corresponding to the dispersion forces approximation divides such region in two subregions. In one of these, the Hamiltonian H describing the molecular interaction is the sum of two London attractors. In the second region, H is the sum of a London attractor and a London *repulsor*, an interaction promoting skew relative orientations between adjacent molecules. As a result, a Hamiltonian in the former region is called *fully attractive*, and *partly repulsive* a Hamiltonian in the latter region. In particular, the quadrupolar projection of some instances of exact excluded-volume interactions [31–34] turn out to be partly repulsive [35].

Both fully attractive and partly repulsive Hamiltonians originate the same sequence of condensed phases [30], and the corresponding phase diagram is in harmony to the one derived by Sonnet *et al.* [26], thus considered as universal. Upon lowering the temperature, the isotropic phase can either undergo a direct transition to the biaxial phase, or an intermediate uniaxial phase can appear in between. Whilst the isotropic-to-uniaxial transition is always first-order, all other transitions can be either first- or second-order, depending on the values of the interaction parameters.

Four scalar order parameters are in general needed to describe a biaxial phase: according to the terminology originally adopted in [26], they are denoted as (S, T, S', T'). Here, S has the same role as Maier and Saupe's original uniaxial parameter [36]. When both T and T' vanish, the phase is uniaxial, when either T or T', or both, are non-zero, the phase is biaxial, with different origins for biaxiality. In fact, when $T \neq 0$ this phase relates with the lack of rotational symmetry in the distribution of the long molecular axis; on the other hand, when $T' \neq 0$ biaxiality arises from a tendency to alignment of the short molecular axes. Similarly, S and S' express different measures of uniaxiality, the latter being correlated with the alignment of the short molecular axes. A certain degree of disorientation in the jungle of notations is due to the fact that different scalar order parameters have been introduced by other authors. However, a rather complete account on the diversity of the notation has recently been presented by Rosso [37], together with a useful conversion rules table.

This paper explores and resumes universal features for the uniaxial-to-biaxial transition within the mean field model employed in previous studies [26,28–30]. Some symmetry properties [29] characterise the interaction, which yields a reduction from four to two of the number of order parameters necessary to describe the whole variety of stable condensed phases [38]. Similar reductions do not appear to apply to a generic interaction.

The results presented complement the universal sequence of stable equilibrium phases [30,38]. Within the region in the parameter space where the interaction Hamiltonian is partly repulsive, the mean-field free energy fails to possess a global minimum in the order parameter space, and the search for the stable phases needs conducting through a minimax principle [30], proposed in a different context by Bogolubov Jr. [39–41].

The class of interaction potentials employed here is outlined in Sec. 2. The mean-field model is briefly recalled in Sec. 3, and the desired unifying features are described in Sec. 4. Main conclusions are summarised in the final Sec. 5.

2. MOLECULAR INTERACTION

We restrict our analysis to biaxial molecules possessing the D_{2h} symmetry, i.e., the same one as a rectangular brick. Let $\boldsymbol{e}$, $\boldsymbol{e}_\perp$, and $\boldsymbol{m}$ denote the axes around which the molecule is invariant under rotations by an angle π (see Fig. 1). As all symmetric, traceless tensors endowed with the D_{2h} symmetry about the molecular axes $(\boldsymbol{e}, \boldsymbol{e}_\perp, \boldsymbol{m})$ can be written as linear combinations of

$$\mathbf{q} := \boldsymbol{m} \otimes \boldsymbol{m} - \frac{1}{3}\mathbf{I} \quad \text{and} \quad \mathbf{b} := \boldsymbol{e} \otimes \boldsymbol{e} - \boldsymbol{e}_\perp \otimes \boldsymbol{e}_\perp, \tag{1}$$

where $\mathbf{I}$ is the identity tensor [37], the anisotropic part of any molecular susceptibility can be written as a linear superposition of these tensors.

In a dispersion model, the assumption that these components interact separately with one another justifies the general form given by Straley [16] to the spatial average of the molecular interaction Hamiltonian. If the two interacting molecules are represented by the pairs of

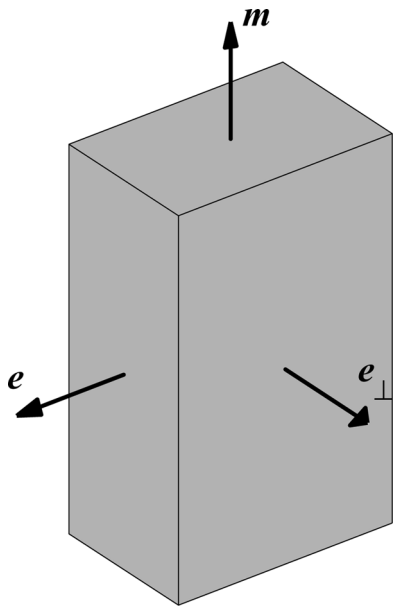

FIGURE 1 A brick is a good picture for a biaxial molecule. $\boldsymbol{e}$, $\boldsymbol{e}_\perp$, and $\boldsymbol{m}$ are the unit vector identifying the directions around which the molecule is invariant under rotations by an angle π; in other words, they are associated with the straight lines orthogonal to the faces of the brick.

tensors $(\mathbf{q}, \mathbf{b})$ and $(\mathbf{q}', \mathbf{b}')$, such Hamiltonian reads as

$$H = -U_0\{\xi \mathbf{q}\cdot\mathbf{q}' + \gamma(\mathbf{q}\cdot\mathbf{b}' + \mathbf{b}\cdot\mathbf{q}') + \lambda \mathbf{b}\cdot\mathbf{b}'\}, \tag{2}$$

where $U_0 > 0$ is a scaling energy, and ξ, γ, and λ are scalar parameters, any of which can be chosen with unit modulus, with no loss of generality. It might seem natural to associate $\boldsymbol{m}$ with the long molecular axis, as this would play the role of the molecular director, for a molecule uniaxial around it, e.g., a cylindrical rod with main axis directed along $\boldsymbol{e}$. In fact, the three molecular axes can have interchangeable roles, and permutations symmetries should be taken into account when swapping the molecular axes names [29]. However, for the sake of simplicity, in this paper $\boldsymbol{m}$ will be the *long molecular axis*, and $\boldsymbol{e}$ and $\boldsymbol{e}_\perp$ will be referred to as the *short molecular axes*. Sticking to [38], one can chose $|\xi| = 1$; therefore, within a permutation of axes and a possible re-scaling of U_0, all different Hamiltonians in Eq. (2) that attain their minimum in the configuration where the interacting molecules lay parallel to one another, side by side, are represented by $\xi = 1$ and (γ, λ) in the *essential* triangle, defined by the inequalities

$$\gamma \geqslant 0, \qquad \lambda \geqslant 0, \qquad 1 - 2\gamma - 3\lambda \geqslant 0 \tag{3}$$

and depicted in Figure 2. In the (γ, λ) plane the essential triangle has vertices in $\mathsf{O} = (0,0)$, $\mathsf{I} = \left(0, \frac{1}{3}\right)$, and $\mathsf{V} = \left(\frac{1}{2}, 0\right)$.

The parabola $\lambda = \gamma^2$ is the locus of points for which Eq. (2) reduces to the Hamiltonian H_0 put forward by Freiser [1,2], in agreement with the classical London dispersion forces approximation:

$$H_0 := -U_0\ \mathbf{a}\cdot\mathbf{a}', \tag{4}$$

where $\mathbf{a} := \mathbf{q} + \gamma\mathbf{b}$ and $\mathbf{a}' := \mathbf{q}' + \gamma\mathbf{b}'$ are the anisotropic parts of the dielectric susceptibility tensors of the interacting molecules. For $\gamma = 0$, H reduces to the Hamiltonian studied in [26] and [28]. In the essential triangle, this special Hamiltonian is represented by the segments OI and IT with $\mathsf{T} = \left(\frac{1}{3}, \frac{1}{9}\right)$, whereas any point of the arc OT along the parabola $\lambda = \gamma^2$ correspond to H_0. Both points O and T are somehow peculiar: while the former corresponds to a Hamiltonian H_0 with $\mathbf{a}$ uniaxial, the latter corresponds to a Hamiltonian H_0 with $\mathbf{a}$ bearing the largest possible biaxiality, as $\det\mathbf{a} = 0$. All other points along the arc OT represent different blends of these pure interaction states.

In Figure 2, the segment PT with $\mathsf{P} = \left(\frac{1}{6}, 0\right)$ is tangent to the dispersion parabola at T.

The arc OT divides the essential triangle into two subregions: in each of them, H can be decomposed in the sum of two terms having

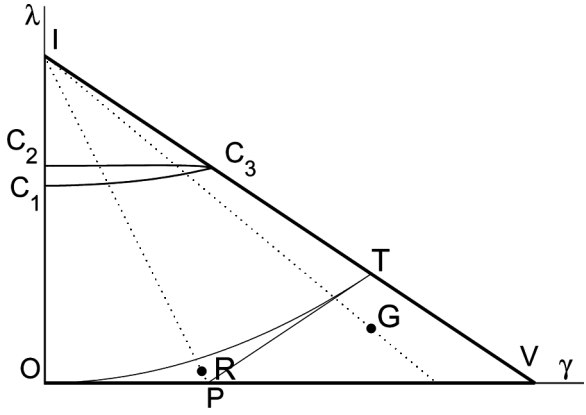

FIGURE 2 The *essential* triangle in the (γ, λ) plane; this region, defined by the inequalities (3), is sufficient to represent all different Hamiltonians in Eq. (2), as long as a permutation of axes and a re-scaling of U_0 are taken into account. The triangle is defined by the positions of the corners: $\mathsf{O} = (0, 0)$, $\mathsf{I} = \left(0, \frac{1}{3}\right)$, and $\mathsf{V} = \left(\frac{1}{2}, 0\right)$. $\mathsf{C}_1\mathsf{C}_3$ is a tricritical line: the corresponding phase diagram exhibits a tricritical point along the uniaxial-to-biaxial transition. $\mathsf{C}_2\mathsf{C}_3$ is a triple line: the corresponding phase diagram exhibits a single direct isotropic-to-biaxial transition, where the isotropic, uniaxial, and biaxial phases are in equilibrium [30]. The limiting points of these lines are positioned in: $\mathsf{C}_1 \simeq (0, 0.20)$, $\mathsf{C}_2 \simeq (0, 0.22)$, and $\mathsf{C}_3 = (5/29, 19/87)$. The arc OT belongs to the London dispersion parabola $\lambda = \gamma^2$. PT is the intersection of the essential triangle with the line tangent to this parabola at T. PT divides the region below the dispersion parabola into two sectors; a point has been chosen within each sector, as illustrated in the text. These points are $\mathsf{R} = \left(\frac{\sqrt{3}}{3} - \frac{5}{12}, \frac{7}{6} - \frac{2\sqrt{3}}{3}\right)$ and $\mathsf{G} = \left(\frac{1}{3}, \frac{1}{18}\right)$.

the same form as H_0 in Eq. (4):

$$H = -U_0\{a^+\mathbf{q}^+ \cdot \mathbf{q}^{+\prime} + a^-\mathbf{q}^- \cdot \mathbf{q}^{-\prime}\}\,; \tag{5}$$

here, $\mathbf{q}^+$ and $\mathbf{q}^-$ are linear combinations of $\mathbf{q}$ and $\mathbf{b}$ depending on both γ and λ. In the region above OT both a^+ and a^- are positive, thus both terms in Eq. (5) are attractive. On the contrary, in the region below the parabola they have opposite sign [30], therefore one term will be attractice and the other repulsive. For this reason, the former region is referred to as *fully attractive*, and the latter as *partly repulsive.* A minimax principle has been proposed and justified in [30] to deal with partly repulsive Hamiltonians within the mean-field approximation; such principle has been adopted for all the results presented here pertaining the same approximation.

3. MEAN-FIELD MODEL

Only the main issues of the mean field model will be given here, as details about its foundations and applications can be found in several other papers [26–28,30,38]. An ensemble of biaxial molecules can show condensed phases which can be represented by two order tensors defined as [26]:

$$\mathbf{Q} := \langle \mathbf{q} \rangle \quad \text{and} \quad \mathbf{B} := \langle \mathbf{b} \rangle, \tag{6}$$

where the ensemble average $\langle \cdots \rangle$ is computed within the mean-field approximation [26,30]. According to their definition, both $\mathbf{Q}$ and $\mathbf{B}$ are symmetric and traceless. If no external distorting cause is present, they share the same eigenframe [37]; their representation can be, therefore:

$$\mathbf{Q} = S\left(\boldsymbol{e}_z \otimes \boldsymbol{e}_z - \frac{1}{3}\mathbf{I}\right) + T(\boldsymbol{e}_x \otimes \boldsymbol{e}_x - \boldsymbol{e}_y \otimes \boldsymbol{e}_y), \tag{7a}$$

$$\mathbf{B} = S'\left(\boldsymbol{e}_z \otimes \boldsymbol{e}_z - \frac{1}{3}\mathbf{I}\right) + T'(\boldsymbol{e}_x \otimes \boldsymbol{e}_x - \boldsymbol{e}_y \otimes \boldsymbol{e}_y). \tag{7b}$$

When both T and T' vanish, the condensed phase described by $\mathbf{Q}$ and $\mathbf{B}$ is uniaxial; however, S and S' have a different meaning, the former being the usual Maier and Saupe's order parameter, i.e., related to the anisotropy in the distribution of main axis $\boldsymbol{m}$, and the latter being related to the anisotropy in the distribution of the other axes $\boldsymbol{e}$ and $\boldsymbol{e}_\perp$. On the other hand, the two parameters T and T' describe biaxiality, and the former characterises the lack of rotational symmetry in the distribution of the long molecular axis $\boldsymbol{m}$, whilst the latter is related to the molecular biaxiality [26,28].

The scalar order parameters (S, T, S', T') must obey four consistency conditions, equivalent to the stationarity conditions for the free energy $\mathcal{F}$ which takes the following form:

$$\mathcal{F} = U_0\left\{\frac{1}{3}S^2 + T^2 + 2\gamma\left(\frac{1}{3}SS' + TT'\right) + \lambda\left(\frac{1}{3}S'^2 + T'^2\right) - \frac{1}{\beta}\ln\left(\frac{Z}{8\pi^2}\right)\right\}, \tag{8}$$

where

$$\frac{1}{\beta} := \frac{k_B t}{U_0} \tag{9}$$

is the reduced temperature, k_B is the Boltzmann constant and Z is the partition function. In the parametrisation of the molecular orientation

adopted in [26], ϑ, φ, and ψ represent the polar angle, the azimuth, and the angle of proper rotation, respectively. In these variables,

$$S = \frac{1}{2}\langle 3\cos^2\vartheta - 1\rangle, \quad S' = \frac{3}{2}\langle \sin^2\vartheta \cos 2\psi\rangle, \tag{10a}$$

$$T = \frac{1}{2}\langle \sin^2\vartheta \cos 2\varphi\rangle, \tag{10b}$$

$$T' = \frac{1}{2}\langle (1+\cos^2\vartheta)\cos 2\varphi\cos 2\psi - 2\cos\vartheta \sin 2\varphi \sin 2\psi\rangle. \tag{10c}$$

Consequently, the scalar order parameters are bounded as follows [26]:

$$-\frac{1}{2} \leqslant S \leqslant 1, -(1-S) \leqslant S' \leqslant (1-S), \tag{11a}$$

$$-\frac{1}{3}(1-S) \leqslant T \leqslant \frac{1}{3}(1-S), \tag{11b}$$

$$\begin{aligned} -\frac{1}{3}\min\{2+S+3T+S', 2+S-3T+S'\} \leqslant T' \\ \leqslant \frac{1}{3}\min\{2+S-3T+S', 2+S+3T-S'\}. \end{aligned} \tag{11c}$$

Equation (10a) show that S' can vanish if the short molecular axes are randomly distributed, even in the presence of a certain degree of orientation of the long axis, expressed by $S > 0$. On the other hand, a certain degree of locking in the short axes distribution would contribute less to S' if the long axis is more aligned. Two different mechanisms contribute to increase S': the locking of the short axes $(\boldsymbol{e}, \boldsymbol{e}_\perp)$ and the widening of the cone described by the long axis $\boldsymbol{m}$ around the uniaxial director $\boldsymbol{e}_z$, which would decrease S. For this reason, in a uniaxial phase the effectiveness of the short axes locking might cause S' to increase as the temperature decreases, and could also be accompanied by a temporary decrease of S. In other words, as we can write

$$S' = \frac{3}{2}(\langle(\boldsymbol{e}\cdot\boldsymbol{e}_z)^2\rangle - \langle(\boldsymbol{e}_\perp\cdot\boldsymbol{e}_z)^2\rangle), \tag{12}$$

an increase in S', measuring the difference in the degree of alignment of the short molecular axes along the uniaxial director, can be associated with a decrease in S, as this would widen the range of variability of both fluctuating quantities in Eq. (12).

Order parameters are often expressed as ensemble averages of symmetry-adapted combinations of Wigner rotation functions R^2_{00}, R^2_{20}, R^2_{02}, and R^2_{22} [15,18,32,45–48]. For comparison purposes, they can be expressed in terms of S, T, S', and T':

$$\langle R^2_{00}\rangle = S, \qquad \langle R^2_{20}\rangle = \sqrt{\frac{3}{2}}T, \tag{13a}$$

$$\langle R^2_{02}\rangle = \frac{1}{\sqrt{6}}S', \qquad \langle R^2_{22}\rangle = \frac{1}{2}T'. \tag{13b}$$

A summary of the sequence of phases that can be encountered in a biaxial nematic liquid crystal according to the model adopted is useful; the essential triangle in Figure 2 is divided into three disjoint regions characterised by a different sequence of equilibrium phases traversed as the temperature decreases. Some special points can be placed on the edges of the essential triangle: these are $\mathsf{C}_1 \simeq (0, 0.20)$, a tricritical point; $\mathsf{C}_2 \simeq (0, 0.22)$, a triple point, and $\mathsf{C}_3 = (5/29, 19/87)$, both a triple and a tricritical point. By adopting a shorthand notation introduced in [42], in such a sequence the isotropic, uniaxial, and biaxial phases are denoted by the symbols $\mathbb{I}$, $\mathbb{U}$, and $\mathbb{B}$, respectively; a first-order transition is denoted by "–" and a second-order transition by "=". With such symbols, in $\mathsf{IC}_2\mathsf{C}_3$ the equilibrium phase sequence is $\mathbb{I} - \mathbb{B}$, i.e., as the temperature decreases an ensemble of biaxial molecules traverses both the isotropic and the biaxial phases, undergoing a first-order transition between the two. Similarly, in $\mathsf{C}_2\mathsf{C}_3\mathsf{C}_1$ the equilibrium phase sequence is $\mathbb{I} - \mathbb{U} - \mathbb{B}$, and in $\mathsf{C}_1\mathsf{C}_3\mathsf{VO}$ it is $\mathbb{I} - \mathbb{U} = \mathbb{B}$. As shown in [30], $\mathsf{C}_2\mathsf{C}_3$ is a line of triple points, while $\mathsf{C}_1\mathsf{C}_3$ is a line of tricritical points.

4. UNIVERSAL FEATURES

The phase diagram drawn in [26,28] for the Hamiltonians along OI and IT comprises all the qualitative features of the equilibrium phase sequences, and so it acquires a universal character. A collective view of the phase transitions predicted by the mean-field model along the universal line OITV can be found in [30] and in [38]. The phase sequences have been obtained by applying the traditional minimum principle for the mean-field free energy to the fully attractive Hamiltonians and an appropriate minimax principle to the partly repulsive Hamiltonians [30]. This minimax principle has been subjected to further scrutiny, by studying the order parameter profiles for two points in the essential triangle, G and R, situated below the dispersion parabola OT. Each

point has been selected in one of the two subregions of OTV that behave differently under the permutation symmetry, namely, OTP and PTV (see Fig. 2). G is in the midpoint of the axis of the triangle PTV; its coordinates are $\mathsf{G} \simeq (0.33, 0.056)$. R is along PI, halfway between P and the intersection of PI with the arc OT; its co-ordinates are $\mathsf{R} \simeq (0.16, 0.012)$.

The order parameter profiles have been obtained from a numerical bifurcation analysis of the equilibrium equations for $\mathcal{F}$, performed with the aid of MATCONT [43], a free software package which integrates into MATLAB [44].

The Hamiltonian described by point G, has been studied; the corresponding order parameters S, T, S', and T' are plotted in Figures 3–6 as functions of the ratio t/t_{NI}, where t is the absolute

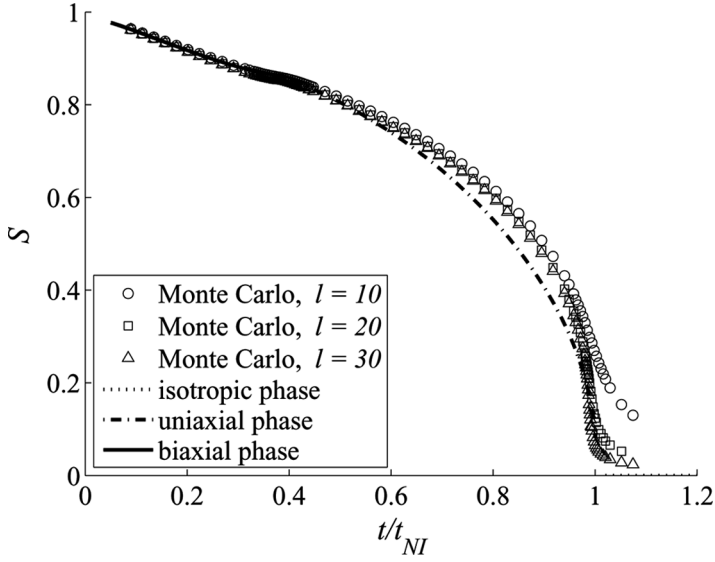

FIGURE 3 The order parameter S, obtained by a mean-field analysis of the Hamiltonian represented by G (see Fig. 2), is plotted as a function of the ratio t/t_{NI}, where t is the absolute temperature and t_{NI} is the value of t that marks the nematic-to-isotropic transition. Monte Carlo simulation results reported here and in the following figures were obtained with three sample sizes, $N = l^3$, with $l = 10,\ 20,\ 30$, represented by circles ◯, squares □, and triangles △, respectively [42]. Temperatures have been scaled to the nematic-isotropic transition temperature. In particular, for mean field data the transition temperature has been obtained from bifurcation analysis of the solutions of the equilibrium problem for Eq. (8), whilst for all three Monte Carlo simulations, t_{NI} is the transition temperature computed for $l = 30$ (see also Table 1).

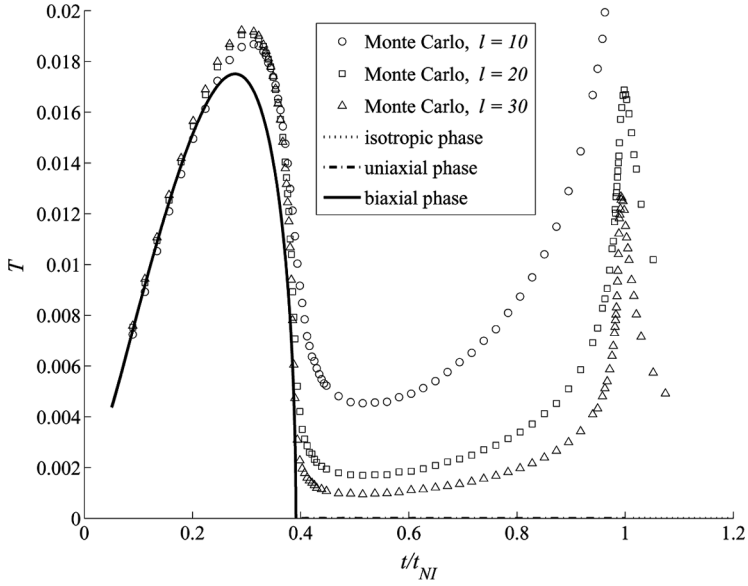

FIGURE 4 The order parameter T, obtained by a mean-field analysis of the Hamiltonian represented by G (see Fig. 2), is plotted as a function of the ratio t/t_{NI}; superimposed to the plot are the corresponding points obtained from a Monte Carlo simulation for different sample sizes, $N = l^3$ (◯: $l = 10$, □: $l = 20$, △: $l = 30$). (For more details, see the caption to Fig. 3). Monte Carlo simulation results around the nematic-to-isotropic transition exhibit a "spurious" spike, whose height decreases with increasing sample size.

temperature and t_{NI} is the value of t that marks the nematic-to-isotropic transition.

A peculiar feature of the plot for S' in Figure 5 draws immediately one's attention: upon reducing the temperature, at the onset of the biaxial phase, S' starts growing again before decreasing towards zero, in agreement with inequalities (11a), as t/t_{NI} further decreases. In the light of the interpretation of the meaning of S', its growth at the biaxial transition can be assumed to be a qualitative measure of the strength of attraction between the short axes. Correspondingly, the plot of S exhibits a dip, as expected. A higher uniaxial rebound at the biaxial transition witnesses a stronger biaxial effectiveness of the molecular interaction and should be associated with a dip more pronounced in the temperature profile of the uniaxial primary order parameter S [42].

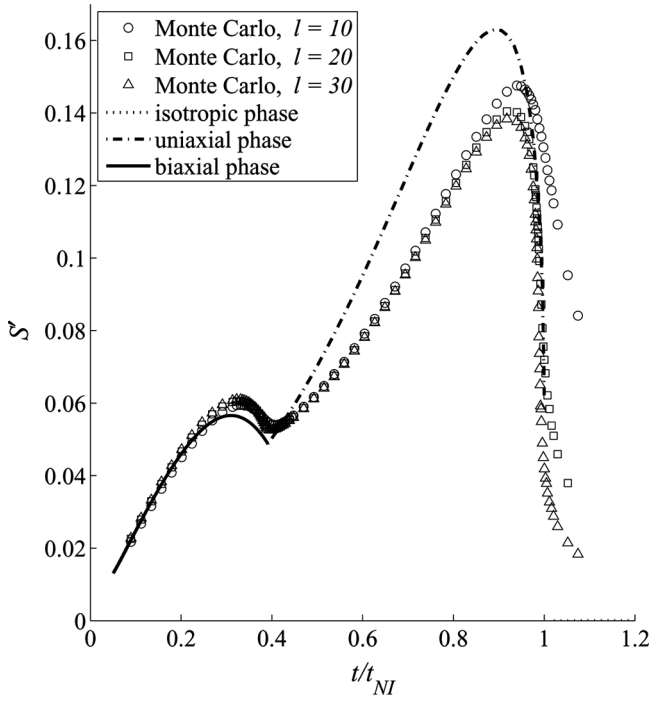

FIGURE 5 The order parameter S', obtained by a mean-field analysis of the Hamiltonian represented by G (see Fig. 2), is plotted as a function of the ratio t/t_{NI}; superimposed to the plot are the corresponding points obtained from a Monte Carlo simulation for different sample sizes, $N = l^3$ (◯: $l = 10$, □: $l = 20$, △: $l = 30$). (For more details, see the caption to Fig. 3). At the onset of the biaxial phase, both the mean-field analysis and the Monte Carlo simulation predict a *rebound* for this order parameter, which is a measure of the strength of attraction between the short molecular axes.

This rebounding behaviour is not characteristic of the point examined, but is indeed a generic feature; in fact, after obtaining the profiles for S' by means of further mean field analysis along the portion of the line IG comprised between the tricritical line and the base of the essential triangle, it has been suggested that such uniaxial rebound at the biaxial transition is indeed a generic feature of all interactions described by the subregion OC_1C_3V of the essential triangle [42].

A similar exploration has been conducted for the point R: the plots for the order parameters S and S' are reported in Figures 7 and 8.

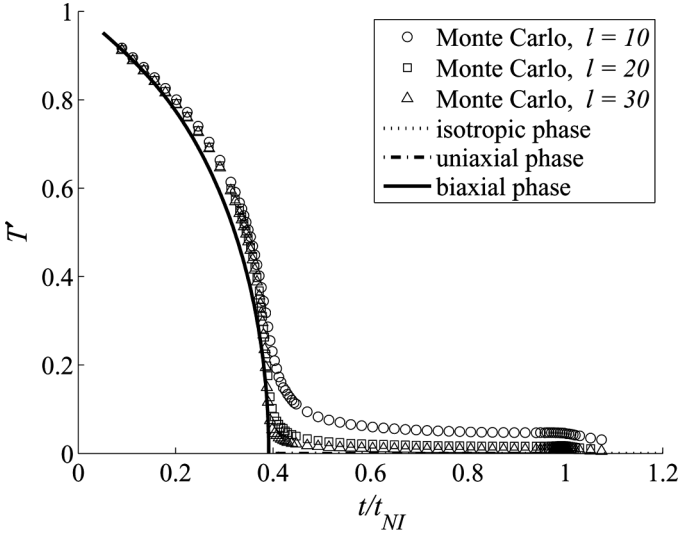

FIGURE 6 The order parameter T', obtained by a mean-field analysis of the Hamiltonian represented by G (see Fig. 2), is plotted as a function of the ratio t/t_{NI}; superimposed to the plot are the corresponding points obtained from a Monte Carlo simulation for different sample sizes, $N = l^3$ (◯: $l = 10$, □: $l = 20$, △: $l = 30$). (For more details, see the caption to Fig. 3).

A uniaxial rebound for S' at the biaxial transition can still be appreciated, although less pronounced.

A wide range analysis of points in the essential triangle along the line IR has confirmed the uniaxial rebound is a property that accompanies the biaxial transition as long as the interaction Hamiltonian fails to be represented by the border OIV of the essential triangle, where two scalar order parameters in general suffice to describe all equilibrium phases [26,28,38]. However, the rebound has different relevance according to the point, i.e., to the specific set of parameters in the molecular interaction potential.

To sum up, the uniaxial rebound at the biaxial transition described above appears as a universal feature accompanying the condensed phases predicted by the most general of Straley's interactions. This property has been predicted for the points G and R in the essential triangle related to a partly repulsive Hamiltonian; in this case, the minimax strategy must be applied to identify the equilibrium order parameters [30]. To ensure that this feature is independent of the mean-field treatment adopted, a Monte Carlo

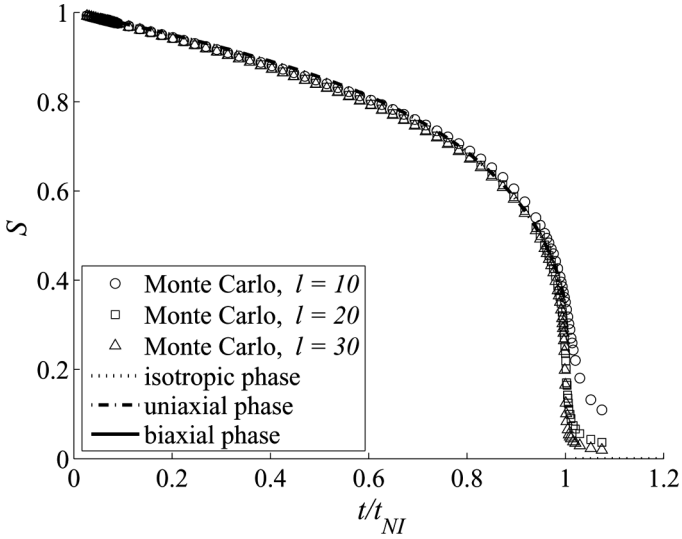

FIGURE 7 The order parameter S, obtained by a mean-field analysis of the Hamiltonian represented by R (see Fig. 2), is plotted as a function of the ratio t/t_{NI}; superimposed to the plot are the corresponding points obtained from a Monte Carlo simulation for different sample sizes, $N = l^3$ (◯: $l = 10$, □: $l = 20$, △: $l = 30$). (For more details, see the caption to Fig. 3).

simulation has been performed [42]; for such simulation, only the interaction molecular potential is retained. In consideration of that, the graphs in Figures 3 to 8 also show the data obtained from this Monte Carlo simulation with different sample sizes: the total number of particles is $N = l^3$, with $l = 10,\ 20,\ 30$, respectively. The four order parameters have been obtained by averaging the appropriate symmetry adapted basis functions defined by Eqs. (10a) to (10c), and computed by complying with methodologies discussed in detail by other Authors [18,22,46–48]; the computational details are available in [42].

Though the values of t_{NI} computed through the mean-field approximation and the Monte Carlo simulation are different, once reduced to the same dimensionless temperature scale t/t_{NI}, the data obtained with the two methods are in a remarkable agreement. In all of the plots, the transition temperature is computed for the largest sample size ($l = 30$) for all three Monte Carlo simulations t_{NI}. To be precise, actual simulations take up a dimensionless temperature scale T^* differing by a factor 9 from the one in Eq. (9). The following mapping

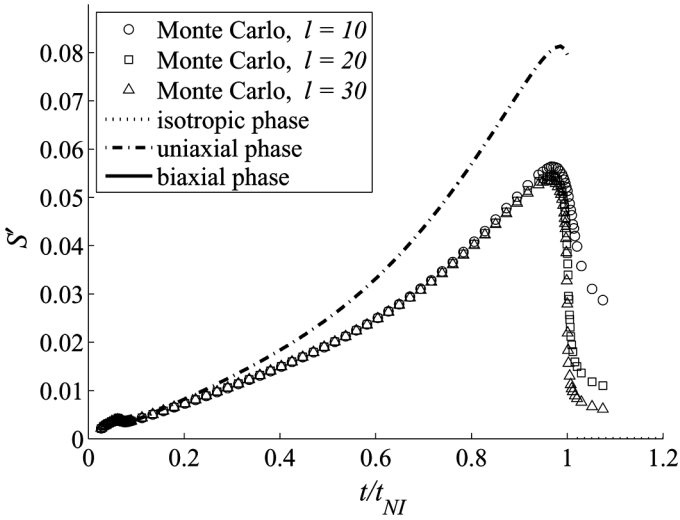

FIGURE 8 The order parameter S', obtained by a mean-field analysis of the Hamiltonian represented by R (see Fig. 2), is plotted as a function of the ratio t/t_{NI}; superimposed to the plot are the corresponding points obtained from a Monte Carlo simulation for different sample sizes, $N = l^3$ (◯: $l = 10$, □: $l = 20$, △: $l = 30$). (For more details, see the caption of Fig. 3). The rebound at the onset of the biaxial phase, predicted both by the mean-field analysis and the Monte Carlo simulation, is less pronounced than in Figure 5, but it is still present.

exists between the temperature scales:

$$T^* = \frac{9}{\beta}, \tag{14}$$

and both mean-field and simulation results have been converted to a single scale for comparisons.

Table 1 lists the critical temperatures in the scale T^* for both the $\mathbb{I} - \mathbb{U}$ and the $\mathbb{U} = \mathbb{B}$ phase transitions, computed within the mean-field approximation and the Monte Carlo simulation for the points R and G in the essential triangle.

In order to estimate how much the parameters (γ, λ) in Eq. (2) affect the physical scenario for the condensed phases, it is expedient an exploration of the ratio $\rho := t_{BU}/t_{NI}$ of the uniaxial-to-biaxial transition temperature to the isotropic-to-uniaxial temperature as a function of (γ, λ) in the region inside the essential triangle (see Fig. 2) where all of the three condensed phases in the scenario are attainable. As no transition to the nematic uniaxial phase is possible

TABLE 1 Transition Temperatures in the T^* Scale (see Eq. (14)) Computed with both Mean-Field and Monte Carlo Treatments for the Hamiltonians Corresponding to the Points R and G in the Essential Triangle (see Fig. 2). $\mathbb{I}-\mathbb{U}$ Denotes a First-Order Isotropic-to-Uniaxial Transition; $\mathbb{U}=\mathbb{B}$ Denotes a Second-Order Uniaxial-to-Biaxial Transition. All of the Monte Carlo Transition Temperatures are Computed for the Largest Sample size, $l=30$

	$\mathbb{I}-\mathbb{U}$		$\mathbb{U}=\mathbb{B}$	
	Mean field	Monte Carlo	Mean field	Monte Carlo
R	1.365 ± 0.004	1.117 ± 0.002	0.111 ± 0.003	0.080 ± 0.001
G	1.560 ± 0.001	1.101 ± 0.002	0.610 ± 0.004	0.428 ± 0.005

above the triple line $\mathsf{C}_2\mathsf{C}_3$, within the essential triangle, t_{NI} is not defined there, and, as a consequence, neither is ρ. On the baseline OV of the triangle no transition to a biaxial phase could be observed, therefore, ρ must vanish. On the other hand, when a point in the triangle approaches the triple line, the two transition temperatures get close to each other, which is equivalent to $\rho \to 1$. In Figure 9 a

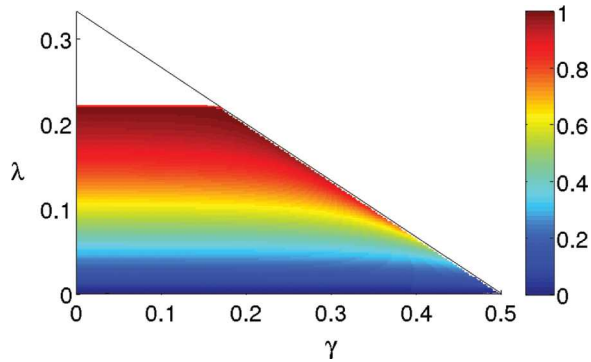

FIGURE 9 A pseudo-colour map of the ratio $\rho := t_{BU}/t_{NI}$ of the uniaxial-to-biaxial transition temperature to the isotropic-to-uniaxial temperature as a function of the (γ, λ) parameters in the interaction potential Eq. (2) in the region inside the essential triangle (see Fig. 2), where all of the three condensed phase involved are attainable. A colourbar is added on the right side of the graph to illustrate the scale. When $\rho \simeq 1$ the two transition temperatures are close to one another, and the corresponding points are therefore close to the triple line $\mathsf{C}_1\mathsf{C}_3$, where $\rho = 1$; when $\rho \simeq 0$, the uniaxial-to-biaxial transition temperature tends to vanish, and the corresponding points are close to the basis OV of the essential triangle.

pseudo-colour map of ρ in the triangle is reported; the colour code, illustrated by a colourbar in the figure, corresponds to dark blue for vanishing ρ, continuously changing into red for $\rho = 1$ through all the rainbow shades. At a glimpse, one can notice how ρ is poorly influenced by γ, whilst it exhibits a strong dependence on λ.

To improve the effectiveness of the representation of this latter exploration, a contour map for ρ is given in Figure 10; the map contains the level sets for a set of linearly spaced values of ρ in the range [0.1,0.9]. In the same map, thicker level curves correspond to compounds which have been claimed capable of thermally driven uniaxial-to-biaxial transitions in the scientific literature. In particular, the curves for the two organo-siloxane tetrapodes used in [8], as well as for the similar germanium compound employed in [10] are drawn. In the first case, infrared spectroscopy measurements indicate for Tetrapode A a ratio $\rho \simeq 0.969$, with a second order transition from the nematic uniaxial phase to the biaxial one, and, for tetrapode B, $\rho \simeq 0.993$, with a first order uniaxial-to-biaxial transition. Similarly,

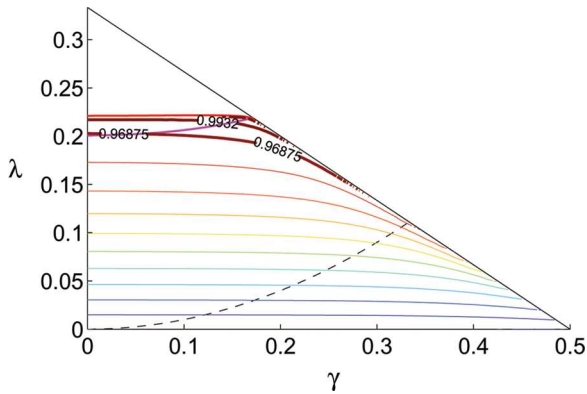

FIGURE 10 A contour map of the ratio $\rho := t_{BU}/t_{NI}$ of the uniaxial-to-biaxial transition temperature to the isotropic-to-uniaxial transition temperature as a function of the (γ, λ) parameters in the interaction potential Eq. (2) in the region inside the essential triangle (see Fig. 2) where all of the three condensed phase involved are attainable. The thin lines correspond to $\rho = 0.1$ to 0.9, with linearly spaced values in that range. The thick lines correspond to the compounds used in [8] (Tetrapode A, $\rho = 0.969$, and Tetrapode B, $\rho = 0.993$), and to the tetrapodal compound used in [10], for which $\rho = 0.999$. A label in the graph allows identifying the level curves for Tetrapode A and B. The colour code for the thin contour lines is the same as in Figure 9.

dynamic light scattering measurements performed on a sample of the germanium tetrapode yield $\rho \simeq 0.999$, revealing weakly first order uniaxial-to-biaxial nematic phase transition. As can be observed in Figure 10, all of the three corresponding level curves cross the tricritical line, therefore each of them is compatible with both a first-order and a second-order uniaxial-to-biaxial transition, the actual type attainable being controlled by the actual value of the (γ, λ) parameters. Details of the exploration, as well as a more thorough assessment of the comparison between the model prediction and the experimental results is given in [49].

5. CONCLUSION

When dealing with the explorations of Straley's general interaction Hamiltonian, it has often been observed that just two scalar order parameters are sufficient to describe the whole sequence of equilibrium condensed phases experienced by an undistorted ensemble of nematogenic biaxial molecules upon decreasing the temperature [1,2,17,26,28]. It has recently been proved [30,38] that this property is a special case, in fact the consequence of a symmetry in Straley's interaction Hamiltonian H in Eq. (2) when the parameters (γ, λ) are chosen along the sides OI and IV of the essential triangle (see Fig. 2). Such reduction is in harmony with the one long been known for the Hamiltonian H_0 in Eq. (4), i.e., on the arc OT along the parabola corresponding to London's dispersion forces approximation [1,2]. Apart from the points on such parabola, no similar reduction has been found for Hamiltonians described in all other points in the internal part of the essential triangle.

A considerable effort has been carried out in order to identify generic macroscopic features common to the whole class of Straley's microscopic interactions, in other words to all of the points in the interior of the essential triangle. One of these feature can be established in the temporary increase of the order parameter S', related to the ensemble average $\langle R^2_{02} \rangle$ of a Wigner symmetry-adapted function, representing the uniaxial component of the biaxial order tensor $\mathbf{B}$ in Eq. (7b).

Although with different degrees of relevance, indeed in all mean-field calculations performed S' rebounds at the biaxial transition and at first it increases again upon decreasing the temperature, whereas in the uniaxial phase it shows a tendency to decrease in the proximity of the transition. A dip in the temperature profile of S is systematically associated with the rebound of S'. In any case, such a

uniaxial rebound is restricted to a temperature range around the transition, as S' must eventually decrease to zero when S saturates towards its maximum value, according to Eq. (11a). However, the rebound seems to persist for all interactions in the interior of the essential triangle.

A Monte Carlo simulation conducted for two partly repulsive Hamiltonians has confirmed mean-field predictions, in particular the uniaxial rebound at the biaxial transition. In consideration of the fact that the Monte Carlo simulation simply rely on the form of the molecular Hamiltonian in Eq. (2) and is not affected by the approximation employed in the mean field approach, the agreement achieved confirms the validity of the minimax principle.

As a consequence of that, the uniaxial rebound at the biaxial transition should be regarded as a generic signature of Straley's interaction: within this theory, its absence is therefore possible only in the presence of further symmetries associated with either sides OI and IV of the essential triangle.

The effect of the Hamiltonian parameters on the temperature governing the phase transitions has been explored, too. In particular, the ratio ρ of the uniaxial-to-biaxial temperature to the isotropic-to-uniaxial temperature has been studied. A poor dependence on γ shows up, as long as the point chosen is not too close to the side IV of the essential triangle. In the light of this, the interpretation of λ as the main biaxial parameter is justified, as well as the initial choice of applying the model for the Hamiltonian (2) with $\gamma = 0$ in [26–28]. This result reassures the interpretation of some experimental results, which has been given by employing inaccurately such model [8]. In fact, a more accurate and thorough analysis might be necessary, performed by choosing the correct set of parameters (γ, λ); however, the outline of the phase transition scenario obtained is compatible with the full model, as the analysis of the level sets for ρ has shown. Further and more detailed study on this issue needs to be performed and will be published.

REFERENCES

[1] Freiser, M. J. (1970). *Phys. Rev. Lett.*, *24*, 1041.
[2] Freiser, M. J. (1971). *Mol. Cryst. Liq. Cryst.*, *14*, 165.
[3] Yu, L. J. & Saupe, A. (1980). *Phys. Rev. Lett.*, *45*, 1000.
[4] Luckhurst, G. R. (2001). *Thin Solid Films*, *393*, 40.
[5] Madsen, L. A., Dingemans, T. J., Nakata, M., & Samulski, E. T. (2004). *Phys. Rev. Lett.*, *92*, 145505.
[6] Acharya, B. R., Primak, A., & Kumar, S. (2004). *Phys. Rev. Lett.*, *92*, 145506.
[7] Severing, K. & Saalwächter, K. (2004). *Phys. Rev. Lett.*, *92*, 125501.

[8] Merkel, K., Kocot, A., Vij, J. K., Korlacki, R., Mehl, G. H., & Meyer, T. (2004). *Phys. Rev. Lett.*, *93*, 237801.
[9] Severing, K., Stibal-Fischer, E., Hasenhindl, A., Finkelmann, H., & Saalwächter, K. (2006). *J. Phys. Chem. B*, *110*, 15680.
[10] Neupane, K., Kang, S. W., Sharma, S., Carney, D., Meyer, T., Mehl, G. H., Allender, D. W., Kumar, S., & Sprunt, S. (2006). *Phys. Rev. Lett.*, *97*, 207802.
[11] Luckhurst, G. R. (2004). *Nature*, *430*, 413.
[12] Luckhurst, G. R. (2005). *Angew. Chem. Int. Ed.*, *44*, 2834.
[13] Galerne, Y. (2006). *Phys. Rev. Lett.*, *96*, 219803.
[14] Madsen, L. A., Dingemans, T. J., Nakata, M., & Samulski, E. T. (2006). *Phys. Rev. Lett.*, *96*, 219804.
[15] Romano, S. (2004). *Physica A*, *337*, 505.
[16] Straley, J. P. (1974). *Phys. Rev. A*, *10*, 1881.
[17] Boccara, N., Mejdani, R., & De Seze, L. (1976). *J. de Phys. (Paris)*, *38*, 149.
[18] Biscarini, F., Chiccoli, C., Pasini, P., Semeria, F., & Zannoni, C. (1995). *Phys. Rev. Lett.*, *75*, 1803.
[19] Israelachvili, J. N. (1992). *Intermolecular and surface forces*, Academic Press: London.
[20] Tjipto–Margo, B. & Evans, G. T. (1991). *J. Chem. Phys.*, *94*, 4546.
[21] Teixeira, P. I. C., Masters, A. J., & Mulder, B. M. (1998). *Mol. Cryst. Liq. Cryst.*, 323, 167.
[22] Allen, M. P. (1990). *Liq. Cryst.*, *8*, 499.
[23] Camp, P. J. & Allen, M. P. (1997). *J. Chem. Phys.*, *106*, 6681.
[24] Camp, P. J., Allen, M. P., & Masters, A. J. (1999). *J. Chem. Phys.*, *111*, 9871.
[25] Bergersen, B. & Palffy-Muhoray, P. (1988). *Liq. Cryst.*, *3*, 347.
[26] Sonnet, A. M., Virga, E. G., & Durand, G. E. (2003). *Phys. Rev. E*, *67*, 061701.
[27] De Matteis, G. & Virga, E. G. (2005). *Phys. Rev. E*, *71*, 061703.
[28] De Matteis, G., Romano, S., & Virga, E. G. (2005). *Phys. Rev. E*, *72*, 041706.
[29] Longa, L., Grzybowski, P., Romano, S., & Virga, E. (2005). *Phys. Rev. E*, *71*, 051714.
[30] Bisi, F., Virga, E. G., Gartland, E. C. Jr., De Matteis, G., Sonnet, A. M., & Durand, G. E. (2006). *Phys. Rev. E*, *73*, 051709.
[31] Mulder, B. M. (1986). *Liq. Cryst.*, *1*, 539.
[32] Mulder, B. (1989). *Phys. Rev. A*, *39*, 360.
[33] Taylor, M. P. (1991). *Liq. Cryst.*, *9*, 141.
[34] Mulder, B. M. (2005). *Mol. Phys.*, *103*, 1411.
[35] Rosso R. & Virga, E. G. (2006). *Phys. Rev. E*, *74*, 021712.
[36] Maier, W. & Saupe, A. (2004). *Z. Naturforsch.*, *14a*, 882 (1959). Translated into English in Sluckin, T. J., Dunmur, D., & Stegemeyer, H. (2004). *Crystals that Flow*, Taylor and Francis: London, 381–385.
[37] Rosso, R. (2007). *Liq. Cryst.*, *34*, 737.
[38] De Matteis, G., Bisi, F., & Virga, E. G. (2007). *Cont. Mech. Thermodyn.*, *19*, 1.
[39] Bogolubov, Jr. N. N. (1972). *A Method for Studying Model Hamiltonians*, Pergamon Press: Oxford.
[40] Osipov, M. A. & Shumovskii, A. S. (1981). *Teor. Mat. Fiz.*, *46*, 125. [(1981). *Theor. Math. Phys.*, *46*, 83].
[41] Bogolubov, N. N. Jr., Sadovnikov, B. I., & Shumosky, A. S. (1994). *Mathematical Methods of Statistical Mechanics of Model Systems*, CRC Press: Boca Raton.
[42] Bisi, F., Romano, S., & Virga, E. G. (2007). *Phys. Rev. E*, *75*, 041705.
[43] See http: //www.matcont.ugent.be/matcont.html
[44] MATLAB is a registered trademark of The MathWorks, Inc. http: //www.mathworks.com

[45] Chiccoli, C., Pasini, P., Semeria, F., & Zannoni, C. (1999). *Int. J. Mod. Phys. C*, *10*, 469.
[46] Zannoni, C. (1979). In: *The molecular physics of liquid crystals*, Luckhurst, G. R. & Gray, G. W. (Eds.), Academic Press: London, Chapters 3 and 9.
[47] Zannoni, C. (2000). NATO Science Series. In: *Advances in the computer simulations of liquid crystals*, Pasini, P. & Zannoni, C. (Eds.), Kluwer: Dordrecht, Vol. C 545, Chapter 2.
[48] Luckhurst, G. R. (2001). In: *Physical properties of liquid crystals: nematics*, Dunmur, D. A., Fukuda, A., & Luckhurst, G. R. (Eds.), INSPEC: London, Chapter 2.1.
[49] Bisi, F., Luckhurst, G. R., & Virga, E. G. (2008). *Phys. Rev. E*, *78*, 021710.